A First-Estimates Jacobian EKF for Improving SLAM Consistency

Guoquan P. Huang[1], Anastasios I. Mourikis[1,2], and Stergios I. Roumeliotis[1]

[1]Dept. of Computer Science and Engineering, University of Minnesota, Minneapolis, MN 55455
[2]Dept. of Electrical Engineering, University of California, Riverside, CA 92521
Email: {ghuang|mourikis|stergios}@cs.umn.edu

Summary. In this work, we study the inconsistency of EKF-based SLAM from the perspective of observability. We analytically prove that when the Jacobians of the system and measurement models are evaluated at the latest state estimates during every time step, the linearized error-state system employed in the EKF has observable subspace of dimension higher than that of the actual, nonlinear, SLAM system. As a result, the covariance estimates of the EKF undergo reduction in directions of the state space where no information is available, which is a primary cause of the inconsistency. Furthermore, a new "First-Estimates Jacobian" (FEJ) EKF is proposed to improve the estimator's consistency during SLAM. The proposed algorithm performs better in terms of consistency, because when the filter Jacobians are calculated using the first-ever available estimates for each state variable, the error-state system model has an observable subspace of the same dimension as the underlying nonlinear SLAM system. The theoretical analysis is validated through both simulations and experiments.

1 Introduction

For autonomous vehicles exploring unknown environments, the ability to perform simultaneous localization and mapping (SLAM) is essential. Among the numerous algorithms developed thus far for the SLAM problem, the extended Kalman filter (EKF) remains one of the most popular ones, and has been used in several practical applications. In this work, we address the *consistency* issue of the EKF-SLAM algorithm, which has recently received considerable attention [1, 2, 3, 4, 5, 6]. As defined in [7], a state estimator is consistent if the estimation errors (i) are zero-mean, and (ii) have covariance matrix smaller or equal to the one calculated by the filter. Consistency is one of the primary criteria for evaluating the performance of any estimator; if an estimator is inconsistent, then the accuracy of the produced state estimates is unknown, which in turn makes the estimator unreliable.

Since SLAM is a nonlinear estimation problem, no provably consistent estimator can be constructed for it. The consistency of every estimator has to be evaluated experimentally. In particular for the *standard* EKF-SLAM algorithm, there exists significant empirical evidence showing that the computed state estimates tend to be *inconsistent*. The first work to draw attention to this issue was that of Julier and Uhlmann [1]. Specifically, in [1] it was observed that when a stationary robot measures the relative position of a new landmark multiple times, the estimated variance of the robot's orientation becomes smaller. Since the observation of a previously unseen feature does not provide any information about the robot's state, this reduction is "artificial," and leads to inconsistency. Bailey *et al.* [4] examined several symptoms of the inconsistency of the standard EKF algorithm, and argued, based on simulation results, that the uncertainty in the robot orientation is the main cause of the inconsistency of EKF-SLAM. The work of [5, 6] further confirmed the empirical findings in [4] and extended the analysis of [1] to the case of a robot that observes a landmark from *two* positions. It is shown that, in this special case, the violation of a certain condition that needs to be satisfied by the filter Jacobians leads to inconsistency. Interestingly, this condition is a special case of (15), which is derived in Section 2.2 for general motion and measurement models.

The aforementioned works have described several symptoms of inconsistency that appear in the standard EKF-SLAM. However, they have not conducted a detailed analysis into the exact cause of inconsistency, for the general case of a moving robot. In this paper, we investigate in depth one of the fundamental causes of inconsistency. In particular, we revisit this problem from a new perspective, i.e., by analyzing the observability properties of the filter's error-state system model. The main contributions of this work are the following:

- Through an observability analysis, we prove that the standard EKF-SLAM employs an error-state system model that has an unobservable subspace of dimension 2, even though the underlying nonlinear system model has 3 unobservable degrees of freedom (corresponding to the position and orientation of the global reference frame). This is a primary cause of filter inconsistency.
- We propose a new algorithm, termed *First Estimates Jacobian* (FEJ)-EKF, which improves the estimator's consistency during SLAM. Specifically, we show analytically that when the EKF Jacobians are computed using the first-ever available estimates for each of the state variables, the error-state model has the *same* observability properties as the underlying nonlinear model. As a result of these properties, the new FEJ-EKF outperforms, in terms of accuracy and consistency, alternative approaches to this problem [3].

In the next section, the observability analysis of SLAM is presented, and it is employed to prove that the standard EKF-SLAM always has "incorrect" ob-

servability properties. Section 3 describes the proposed FEJ-EKF algorithm, and in Section 4 the performance of this new estimator is compared with that of existing solutions [3] through Monte Carlo simulations and experiments. Finally, Section 5 outlines the main conclusions of this work.

2 SLAM Observability Analysis

The observability properties of SLAM have been studied in only few cases in the literature. In particular, [8, 9] investigated the observability of a simple *linear time-invariant* (LTI) SLAM system, and showed that it is unobservable. On the other hand, in [10] the observability of the nonlinear SLAM system was studied, using the nonlinear observability rank condition developed by Hermann and Krener [11]. This work proved that the nonlinear SLAM system is unobservable, with 3 unobservable degrees of freedom corresponding to the global position and orientation of the state vector. However, to the best of our knowledge, an analysis of the observability properties of the EKF *linearized* error-state system model does not exist to date. This is an important omission, since this model is the one that is actually used in practice, and thus its observability properties affect the performance of the estimator. In particular, in this paper we show that these properties play a significant role in determining the consistency of the filter.

In the following, after presenting the equations of the EKF-SLAM formulation with *generalized* system and measurement models, we examine the observability properties of the EKF's linearized error-state system. This analysis constitutes an important generalization of previous works, that either considered the special cases of a robot observing a landmark from one or two poses [1, 5, 6], or imposed limitations on the types of robot-to-landmark measurements admissible [12]. Based on this analysis, we draw conclusions about the consistency of the filter. To preserve the clarity of the presentation, in this section we consider the case where a *single* landmark is included in the state vector. However, the conclusions drawn in this case can be readily extended to the general case of multiple landmarks. We note that, due to space limitations, some intermediate steps of the derivations have been omitted, and the interested reader is referred to [13] for details.

2.1 Standard EKF-SLAM

In the standard formulation of SLAM, the state vector comprises the robot pose and the landmark's position in the global frame. Thus, at time-step k the state vector is given by

$$\mathbf{x}_k^T = \begin{bmatrix} \mathbf{p}_{R_k}^T & \phi_{R_k} & \mathbf{p}_L^T \end{bmatrix} = \begin{bmatrix} \mathbf{x}_{R_k}^T & \mathbf{p}_L^T \end{bmatrix} \tag{1}$$

where $\mathbf{x}_{R_k}^T = \begin{bmatrix} \mathbf{p}_{R_k}^T & \phi_{R_k} \end{bmatrix}$ denotes the robot pose (position and orientation), and $\mathbf{p}_L$ is the landmark position. EKF-SLAM recursively evolves in two steps:

propagation and update, based on the discrete-time process and measurement models, respectively.

EKF Propagation

In the propagation step, the robot's odometry measurements are processed to obtain an estimate of the pose change between two consecutive time steps, and then employed in the EKF to propagate the robot state estimate. On the other hand, since the landmark is static, its state estimate does not change with the incorporation of a new odometry measurement. The EKF propagation equations are given by:[1]

$$\hat{\mathbf{p}}_{R_{k+1|k}} = \hat{\mathbf{p}}_{R_{k|k}} + \mathbf{C}(\hat{\phi}_{R_{k|k}})\, {}^{R_k}\hat{\mathbf{p}}_{R_{k+1}} \tag{2}$$

$$\hat{\phi}_{R_{k+1|k}} = \hat{\phi}_{R_{k|k}} + {}^{R_k}\hat{\phi}_{R_{k+1}} \tag{3}$$

$$\hat{\mathbf{p}}_{L_{k+1|k}} = \hat{\mathbf{p}}_{L_{k|k}} \tag{4}$$

where $\mathbf{C}(\cdot)$ denotes 2×2 rotation matrix, and ${}^{R_k}\hat{\mathbf{x}}_{R_{k+1}} = [{}^{R_k}\hat{\mathbf{p}}_{R_{k+1}}^T \;\; {}^{R_k}\hat{\phi}_{R_{k+1}}]^T$ is the odometry-based estimate of the robot's motion between time-steps k and $k+1$. This estimate is corrupted by zero-mean, white Gaussian noise $\mathbf{w}_k = {}^{R_k}\mathbf{x}_{R_{k+1}} - {}^{R_k}\hat{\mathbf{x}}_{R_{k+1}}$, with covariance matrix $\mathbf{Q}_k$.

In addition to the state propagation equations, the linearized error-state propagation equation is necessary for the EKF. This is given by:

$$\tilde{\mathbf{x}}_{k+1|k} = \begin{bmatrix} \mathbf{\Phi}_{R_k} & \mathbf{0}_{3\times 2} \\ \mathbf{0}_{2\times 3} & \mathbf{I}_2 \end{bmatrix} \begin{bmatrix} \tilde{\mathbf{x}}_{R_{k|k}} \\ \tilde{\mathbf{x}}_{L_{k|k}} \end{bmatrix} + \begin{bmatrix} \mathbf{G}_{R_k} \\ \mathbf{0}_{2\times 2} \end{bmatrix} \mathbf{w}_k \triangleq \mathbf{\Phi}_k \tilde{\mathbf{x}}_{k|k} + \mathbf{G}_k \mathbf{w}_k \tag{5}$$

where $\mathbf{\Phi}_{R_k}$ and $\mathbf{G}_{R_k}$ are obtained from the state propagation equations (2)-(3).

$$\mathbf{\Phi}_{R_k} = \begin{bmatrix} \mathbf{I}_2 & \mathbf{J}\mathbf{C}(\hat{\phi}_{R_{k|k}})\, {}^{R_k}\hat{\mathbf{p}}_{R_{k+1}} \\ \mathbf{0}_{1\times 2} & 1 \end{bmatrix} \equiv \begin{bmatrix} \mathbf{I}_2 & \mathbf{J}\left(\hat{\mathbf{p}}_{R_{k+1|k}} - \hat{\mathbf{p}}_{R_{k|k}}\right) \\ \mathbf{0}_{1\times 2} & 1 \end{bmatrix} \tag{6}$$

$$\mathbf{G}_{R_k} = \begin{bmatrix} \mathbf{C}(\hat{\phi}_{R_{k|k}}) & \mathbf{0}_{2\times 1} \\ \mathbf{0}_{1\times 2} & 1 \end{bmatrix} \tag{7}$$

where $\mathbf{J} \triangleq \begin{bmatrix} 0 & -1 \\ 1 & 0 \end{bmatrix}$. It is important to point out that the form of the propagation equations presented above is general, and holds for any robot kinematic model (e.g., unicycle, bicycle, or Ackerman model) [12].

[1] Throughout this paper the subscript $\ell|j$ refers to the estimate of a quantity at time-step ℓ, after all measurements up to time-step j have been processed. $\hat{x}$ is used to denote the estimate of a random variable x, while $\tilde{x} = x - \hat{x}$ is the error in this estimate. $\mathbf{0}_{m\times n}$ and $\mathbf{1}_{m\times n}$ denote $m \times n$ matrices of zeros and ones, respectively, while $\mathbf{I}_n$ is the $n\times n$ identity matrix. Finally, we use the concatenated forms $s\phi$ and $c\phi$ to denote the $\sin\phi$ and $\cos\phi$ functions, respectively.

EKF Update

The measurement used for updates in the EKF is a function of the relative position of the landmark with respect to the robot:

$$\mathbf{z}_k = \mathbf{h}(\mathbf{x}_k) + \mathbf{v}_k = \mathbf{h}\left({}^{R_k}\mathbf{p}_L\right) + \mathbf{v}_k \tag{8}$$

where ${}^{R_k}\mathbf{p}_L = \mathbf{C}^T(\phi_{R_k})(\mathbf{p}_L - \mathbf{p}_{R_k})$ is the position of the landmark with respect to the robot at time-step k, and $\mathbf{v}_k$ is zero-mean Gaussian measurement noise with covariance $\mathbf{R}_k$. In this work, we allow $\mathbf{h}$ to describe *any* measurement model, such as a direct measurement of relative position, a pair of range and bearing measurements, bearing-only or distance-only measurements, etc. Generally, the measurement function $\mathbf{h}$ is nonlinear, and hence it is linearized for use in the EKF. The linearized measurement-error equation is given by

$$\tilde{\mathbf{z}}_k \simeq \begin{bmatrix}\mathbf{H}_{R_k} & \mathbf{H}_{L_k}\end{bmatrix} \begin{bmatrix}\tilde{\mathbf{x}}_{R_{k|k-1}} \\ \tilde{\mathbf{x}}_{L_{k|k-1}}\end{bmatrix} + \mathbf{v}_k \triangleq \mathbf{H}_k \tilde{\mathbf{x}}_{k|k-1} + \mathbf{v}_k \tag{9}$$

where $\mathbf{H}_{R_k}$ and $\mathbf{H}_{L_k}$ are the Jacobians of $\mathbf{h}$ with respect to the robot pose and the landmark position, respectively, evaluated at the state estimate $\hat{\mathbf{x}}_{k|k-1}$. Using the chain rule of differentiation, these are computed as:

$$\mathbf{H}_{R_k} = (\nabla \mathbf{h}_k)\mathbf{C}^T(\hat{\phi}_{R_{k|k-1}}) \begin{bmatrix}-\mathbf{I}_2 & -\mathbf{J}(\hat{\mathbf{p}}_{L_{k|k-1}} - \hat{\mathbf{p}}_{R_{k|k-1}})\end{bmatrix} \tag{10}$$

$$\mathbf{H}_{L_k} = (\nabla \mathbf{h}_k)\mathbf{C}^T(\hat{\phi}_{R_{k|k-1}}) \tag{11}$$

where $\nabla \mathbf{h}_k$ denotes the Jacobian of $\mathbf{h}$ with respect to the robot-relative landmark position ${}^{R_k}\mathbf{p}_L$, evaluated at the state estimate $\hat{\mathbf{x}}_{k|k-1}$.

2.2 EKF-SLAM Observability Analysis

It is well-known (cf. [10, 13]) that the underlying physical system in SLAM has 3 unobservable degrees of freedom, corresponding to the *global* coordinates of the state vector (rotation and translation). Thus, when the EKF is used for state estimation in SLAM, we would expect that the system model employed by the EKF also shares this property. However, in this section we show that this is not the case, since the unobservable subspace of the linearized error-state model of the standard EKF is generally of dimension only 2.

Since the linearized error-state model for EKF-SLAM is time-varying, we employ the *local observability matrix* [14] to perform the observability analysis. Specifically, for the EKF-SLAM system considered in this work (cf. (5) and (9)), the local observability matrix for the time interval between time-steps k and $k+m$ is defined as:

$$\mathbf{M} \triangleq \begin{bmatrix}\mathbf{H}_k \\ \mathbf{H}_{k+1}\mathbf{\Phi}_k \\ \vdots \\ \mathbf{H}_{k+m}\mathbf{\Phi}_{k+m-1}\cdots\mathbf{\Phi}_k\end{bmatrix} = \begin{bmatrix}\mathbf{H}_{R_k} & \mathbf{H}_{L_k} \\ \mathbf{H}_{R_{k+1}}\mathbf{\Phi}_{R_k} & \mathbf{H}_{L_{k+1}} \\ \vdots & \vdots \\ \mathbf{H}_{R_{k+m}}\mathbf{\Phi}_{R_{k+m-1}}\cdots\mathbf{\Phi}_{R_k} & \mathbf{H}_{L_{k+m}}\end{bmatrix} \tag{12}$$

Ideal EKF-SLAM

Before considering the rank of the matrix $\mathbf{M}$, which is constructed using the *estimated* values of the state in the filter Jacobians, it is interesting to study the observability properties of the "oracle", or "ideal" EKF (i.e., the filter whose Jacobians are evaluated using the *true* values of the state variables). In the following, all matrices evaluated using the true state values are denoted by the symbol " $\breve{}$ ".

We start by noting that (cf. (6)):

$$\breve{\mathbf{\Phi}}_{R_{k+1}}\breve{\mathbf{\Phi}}_{R_k} = \begin{bmatrix} \mathbf{I}_2 & \mathbf{J}\left(\mathbf{p}_{R_{k+2}} - \mathbf{p}_{R_k}\right) \\ \mathbf{0}_{1\times 2} & 1 \end{bmatrix} \tag{13}$$

Based on this property, it is easy to show by induction that:

$$\breve{\mathbf{\Phi}}_{R_{k+i-1}}\breve{\mathbf{\Phi}}_{R_{k+i-2}}\cdots\breve{\mathbf{\Phi}}_{R_k} = \begin{bmatrix} \mathbf{I}_2 & \mathbf{J}\left(\mathbf{p}_{R_{k+i}} - \mathbf{p}_{R_k}\right) \\ \mathbf{0}_{1\times 2} & 1 \end{bmatrix} \tag{14}$$

which holds for all $i > 0$. Using this result, and substituting for the measurement Jacobians from (10) and (11), we can prove the following useful identity:

$$\breve{\mathbf{H}}_{R_{k+i}}\breve{\mathbf{\Phi}}_{R_{k+i-1}}\cdots\breve{\mathbf{\Phi}}_{R_k} = (\nabla\breve{\mathbf{h}}_{k+i})\mathbf{C}^T(\breve{\phi}_{R_{k+i}})\left[-\mathbf{I}_2\ -\mathbf{J}(\mathbf{p}_L - \mathbf{p}_{R_k})\right] \tag{15}$$

which holds for all $i > 0$. The matrix $\breve{\mathbf{M}}$ can now be written as

$$\begin{aligned}\breve{\mathbf{M}} =& \underbrace{\mathbf{Diag}\left((\nabla\breve{\mathbf{h}}_k)\mathbf{C}^T(\breve{\phi}_{R_k}),\ \cdots,(\nabla\breve{\mathbf{h}}_{k+m})\mathbf{C}^T(\breve{\phi}_{R_{k+m}})\right)}_{\breve{\mathbf{D}}} \\ & \times \underbrace{\begin{bmatrix} -\mathbf{I}_2\ -\mathbf{J}(\mathbf{p}_L - \mathbf{p}_{R_k})\ \mathbf{I}_2 \\ -\mathbf{I}_2\ -\mathbf{J}(\mathbf{p}_L - \mathbf{p}_{R_k})\ \mathbf{I}_2 \\ \vdots \qquad\qquad \vdots \\ -\mathbf{I}_2\ -\mathbf{J}(\mathbf{p}_L - \mathbf{p}_{R_k})\ \mathbf{I}_2 \end{bmatrix}}_{\breve{\mathbf{N}}}\end{aligned} \tag{16}$$

Lemma 2.1 *The rank of the observability matrix of the ideal EKF,* $\breve{\mathbf{M}}$*, is 2.*

Proof. The rank of the product of the matrices $\breve{\mathbf{D}}$ and $\breve{\mathbf{N}}$ is given by (cf. Eq. (4.5.1) in [15]), $\text{rank}(\breve{\mathbf{D}}\breve{\mathbf{N}}) = \text{rank}(\breve{\mathbf{N}}) - \dim(\mathcal{N}(\breve{\mathbf{D}})\bigcap\mathcal{R}(\breve{\mathbf{N}}))$. Since $\breve{\mathbf{N}}$ is comprised of m repetitions of the same 2×5 block row, it is clear that $\text{rank}(\breve{\mathbf{N}}) = 2$, and the range of $\breve{\mathbf{N}}$, $\mathcal{R}(\breve{\mathbf{N}})$ is spanned by the vectors $\mathbf{u}_1$ and $\mathbf{u}_2$, defined as follows:

$$\begin{bmatrix}\mathbf{u}_1\ \mathbf{u}_2\end{bmatrix} = \begin{bmatrix}\mathbf{I}_2 \\ \mathbf{0}_{3\times 2}\end{bmatrix} \tag{17}$$

We now observe that in general $\breve{\mathbf{D}}\mathbf{u}_i \neq \mathbf{0}$, for $i = 1, 2$. Moreover, note that any vector $\mathbf{x} \in \mathcal{R}(\breve{\mathbf{N}}) \setminus \mathbf{0}$ can be written as $\mathbf{x} = \alpha_1\mathbf{u}_1 + \alpha_2\mathbf{u}_2$ for some $\alpha_1, \alpha_2 \in \mathbb{R}$,

where α_1 and α_2 are not simultaneously equal to zero. Thus, we see that in general $\breve{\mathbf{D}}\mathbf{x} = \alpha_1\breve{\mathbf{D}}\mathbf{u}_1 + \alpha_2\breve{\mathbf{D}}\mathbf{u}_2 \neq \mathbf{0}$, which implies that $\mathbf{x}$ does not belong to the nullspace of $(\breve{\mathbf{D}})$. Therefore, $\dim(\mathcal{N}(\breve{\mathbf{D}}) \bigcap \mathcal{R}(\breve{\mathbf{N}})) = 0$, and, finally, $\text{rank}(\breve{\mathbf{M}}) = \text{rank}(\breve{\mathbf{N}}) - \dim(\mathcal{N}(\breve{\mathbf{D}}) \bigcap \mathcal{R}(\breve{\mathbf{N}})) = \text{rank}(\breve{\mathbf{N}}) = 2$.

The result of the above lemma indicates that when the Jacobians of the EKF are evaluated at true values of the states, the EKF system model has 3 unobservable degrees of freedom. This agrees with intuition, which dictates that the *global coordinates* of the state vector in SLAM (rotation and translation) are unobservable. Moreover, in [13] it is shown that the unobservable subspace of the system model employed by the ideal EKF (i.e., the nullspace of $\breve{\mathbf{M}}$) is *identical* to the nullspace of the observability matrix of the underlying, nonlinear SLAM system. Unfortunately, as shown in the next section, these desirable properties are not shared by the linearized EKF system model, when the Jacobians are evaluated at the latest state estimates.

Standard EKF-SLAM

We now study the observability properties of the standard EKF-SLAM, in which the Jacobians are evaluated at the estimated state. We start by deriving an expression analogous to that of (14). We obtain [12]:

$$\mathbf{\Phi}_{R_{k+i-1}}\mathbf{\Phi}_{R_{k+i-2}}\cdots\mathbf{\Phi}_{R_k} = \begin{bmatrix} \mathbf{I}_2 & \mathbf{J}\left(\hat{\mathbf{p}}_{R_{k+i|k+i-1}} - \hat{\mathbf{p}}_{R_{k|k}} - \sum_{j=k+1}^{k+i-1}\Delta\mathbf{p}_{R_j}\right) \\ \mathbf{0}_{1\times 2} & 1 \end{bmatrix}$$

where $\Delta\mathbf{p}_{R_i} = \hat{\mathbf{p}}_{R_{i|i}} - \hat{\mathbf{p}}_{R_{i|i-1}}$ is the correction in the robot position due to the update at time-step i. Therefore,

$$\mathbf{H}_{R_{k+i}}\mathbf{\Phi}_{R_{k+i-1}}\cdots\mathbf{\Phi}_{R_k} =$$
$$(\nabla\mathbf{h}_{k+i})\mathbf{C}^T(\hat{\phi}_{R_{k+i|k+i-1}}) \times \left[-\mathbf{I}_2\ -\mathbf{J}\left(\hat{\mathbf{p}}_{L_{k+i|k+i-1}} - \hat{\mathbf{p}}_{R_{k|k}} + \sum_{j=k+1}^{k+i-1}\Delta\mathbf{p}_{R_j}\right)\right]$$

Using this result, we can write matrix $\mathbf{M}$ as:

$$\mathbf{M} = \underbrace{\mathbf{Diag}\left((\nabla\mathbf{h}_k)\mathbf{C}^T(\hat{\phi}_{R_{k|k-1}}), \cdots, (\nabla\mathbf{h}_{k+m})\mathbf{C}^T(\hat{\phi}_{R_{k+m|k+m-1}})\right)}_{\mathbf{D}}$$
$$\times \underbrace{\begin{bmatrix} -\mathbf{I}_2 & -\mathbf{J}\left(\hat{\mathbf{p}}_{L_{k|k-1}} - \hat{\mathbf{p}}_{R_{k|k-1}}\right) & \mathbf{I}_2 \\ -\mathbf{I}_2 & -\mathbf{J}\left(\hat{\mathbf{p}}_{L_{k+1|k}} - \hat{\mathbf{p}}_{R_{k|k}}\right) & \mathbf{I}_2 \\ -\mathbf{I}_2 & -\mathbf{J}\left(\hat{\mathbf{p}}_{L_{k+2|k+1}} - \hat{\mathbf{p}}_{R_{k|k}} + \Delta\mathbf{p}_{R_{k+1}}\right) & \mathbf{I}_2 \\ \vdots & \vdots & \vdots \\ -\mathbf{I}_2 & -\mathbf{J}\left(\hat{\mathbf{p}}_{L_{k+i|k+i-1}} - \hat{\mathbf{p}}_{R_{k|k}} + \sum_{j=k+1}^{k+i-1}\Delta\mathbf{p}_{R_j}\right) & \mathbf{I}_2 \end{bmatrix}}_{\mathbf{N}}$$

Lemma 2.2 *The rank of the observability matrix of the system model of the standard EKF,* $\mathbf{M}$*, is equal to 3.*

Proof. First, we note that the estimates of any given state variable at different time instants are generally different. Hence, the following inequalities generally hold $\forall i \neq \ell$: $\hat{\mathbf{p}}_{R_{k+i|k+i-1}} \neq \hat{\mathbf{p}}_{R_{k+i|k+i}}$ and $\hat{\mathbf{p}}_{L_{k+i|k+i-1}} \neq \hat{\mathbf{p}}_{L_{k+\ell|k+\ell-1}}$ Therefore, the third column of $\mathbf{N}$ will be, in general, a vector with unequal elements, and hence $\text{rank}(\mathbf{N}) = 3$. Proceeding similarly to the proof of Lemma 2.1, we first find one possible basis for the range space of $\mathbf{N}$, $\mathcal{R}(\mathbf{N})$. By inspection, we see that such a basis is given simply by the first 3 columns of $\mathbf{N}$, which we denote by $\mathbf{u}_i$ $(i = 1, 2, 3)$. Moreover, it can be verified that generally $\mathbf{D}\mathbf{u}_i \neq \mathbf{0}, \forall i = 1, 2, 3$. Therefore, $\dim(\mathcal{N}(\mathbf{D}) \bigcap \mathcal{R}(\mathbf{N})) = 0$, and finally $\text{rank}(\mathbf{M}) = \text{rank}(\mathbf{N}) - \dim(\mathcal{N}(\mathbf{D}) \bigcap \mathcal{R}(\mathbf{N})) = \text{rank}(\mathbf{N}) = 3$.

We thus see that the linearized error-state model employed in the standard EKF-SLAM has different observability properties than the ideal EKF-SLAM and the underlying nonlinear system. In particular, by processing the measurements collected in the interval $[k, k+m]$, the EKF acquires information in 3 dimensions of the state space (along the directions corresponding to the observable subspace of the EKF). However, the measurements actually provide information in only 2 directions of the state space, and as a result, the EKF gains "spurious information" along the unobservable directions of the underlying nonlinear SLAM system, which leads to inconsistency.

To probe further, we note that the basis of the right nullspace of $\mathbf{M}$ is given by:

$$\mathcal{N}(\mathbf{M}) = \text{span}\left\{ \begin{bmatrix} 1 \\ 0 \\ 0 \\ 1 \\ 0 \end{bmatrix}, \begin{bmatrix} 0 \\ 1 \\ 0 \\ 0 \\ 1 \end{bmatrix} \right\} = \text{span}\left\{ \mathbf{n}_x \ , \ \mathbf{n}_y \right\} \tag{18}$$

Note that these two vectors correspond to a shifting of the $x-y$ plane, which implies that such a shifting is unobservable. On the other hand, we point out that the direction corresponding to the global orientation is "missing" from the unobservable subspace of the EKF system model. Therefore, we see that the filter will gain "nonexistent" information about the robot's global orientation. This will lead to an unjustified reduction in the orientation uncertainty, which will, in turn, further reduce the uncertainty in all the state variables. This agrees in some respects with [4, 6], where it was argued that the orientation uncertainty is the cause of the filter's inconsistency in SLAM. However, we point out that the *root cause* of the problem is the fact that the Jacobians are evaluated at different linearization points at every time step. This changes the dimension of the observable subspace, and thus fundamentally alters the properties of the estimation process.

An additional interesting point is that the covariance matrix of the measurements does not appear in the observability analysis of the filter. Therefore, even if this covariance matrix is artificially inflated, the filter will retain the same observability properties (i.e., the same observable and unobservable subspaces). This shows that no amount of covariance inflation can result in correct

observability properties. Similarly, even if the Iterated EKF is employed for state estimation, the same, erroneous, observability properties will arise, since the landmark position estimates will generally differ at different time steps.

3 First-Estimates Jacobian EKF SLAM

Careful observation of the matrix $\mathbf{M}$ in (21) reveals that it is possible to obtain an EKF system model with an unobservable subspace of dimension 3, even if the Jacobians are not evaluated at the true state values. For this purpose, the following two changes are necessary.

1. In the computation of the state-propagation Jacobian matrix $\mathbf{\Phi}_{R_k}$, we employ the robot position estimate prior to updating, $\hat{\mathbf{p}}_{R_{k|k-1}}$, instead of the updated one, $\hat{\mathbf{p}}_{R_{k|k}}$, as in the standard EKF:
$$\mathbf{\Phi}'_{R_k} = \begin{bmatrix} \mathbf{I}_2 & \mathbf{J}\left(\hat{\mathbf{p}}_{R_{k+1|k}} - \hat{\mathbf{p}}_{R_{k|k-1}}\right) \\ \mathbf{0}_{1\times 2} & 1 \end{bmatrix} \tag{19}$$
2. In the evaluation of the measurement Jacobian matrix $\mathbf{H}_{R_k}$, we always utilize the landmark estimate *from the first time* the landmark was detected. Thus, if a landmark was first seen at time-step ℓ, we compute the measurement Jacobian with respect to the robot pose as:
$$\mathbf{H}'_{R_k} = (\nabla \mathbf{h}_k)\mathbf{C}^T(\hat{\phi}_{R_{k|k-1}}) \left[-\mathbf{I}_2 \; -\mathbf{J}(\hat{\mathbf{p}}_{L_{\ell|\ell}} - \hat{\mathbf{p}}_{R_{k|k-1}})\right] \tag{20}$$

As a result of the above modifications, only the *first* estimates of all landmark positions and all robot poses appear in the Jacobians of the filter. This has an effect that the observability matrix $\mathbf{M}$ of this new filter, which we term *First-Estimates Jacobian* (FEJ)-EKF, assumes the form:

$$\begin{aligned} \mathbf{M}' =& \mathbf{Diag}\left((\nabla \mathbf{h}_k)\mathbf{C}^T(\hat{\phi}_{R_{k|k-1}}), \cdots, (\nabla \mathbf{h}_{k+m})\mathbf{C}^T(\hat{\phi}_{R_{k+m|k+m-1}})\right) \\ & \times \begin{bmatrix} -\mathbf{I}_2 & -\mathbf{J}\left(\hat{\mathbf{p}}_{L_{\ell|\ell}} - \hat{\mathbf{p}}_{R_{k|k-1}}\right) & \mathbf{I}_2 \\ -\mathbf{I}_2 & -\mathbf{J}\left(\hat{\mathbf{p}}_{L_{\ell|\ell}} - \hat{\mathbf{p}}_{R_{k|k-1}}\right) & \mathbf{I}_2 \\ -\mathbf{I}_2 & -\mathbf{J}\left(\hat{\mathbf{p}}_{L_{\ell|\ell}} - \hat{\mathbf{p}}_{R_{k|k-1}}\right) & \mathbf{I}_2 \\ \vdots & \vdots & \vdots \\ -\mathbf{I}_2 & -\mathbf{J}\left(\hat{\mathbf{p}}_{L_{\ell|\ell}} - \hat{\mathbf{p}}_{R_{k|k-1}}\right) & \mathbf{I}_2 \end{bmatrix} \end{aligned} \tag{21}$$

The fact that the rank of this matrix is 2 can be easily proven, by a procedure completely analogous to that of Lemma 2.1. Thus, the FEJ-EKF is based on an error-state system model whose unobservable subspace is of dimension 3. We stress that the FEJ-EKF estimator is realizable in practice, since it does *not* utilize any knowledge of the true state. Interestingly, even though this new filter does not use the latest available state estimates (and thus utilizes Jacobians that are less accurate than those of the standard EKF), it exhibits better consistency properties than the standard EKF, as shown in the following section.

4 Results

In order to validate the preceding theoretical analysis and to demonstrate the capability of the FEJ-EKF filter to improve the consistency of EKF-SLAM, a series of Monte Carlo simulation tests and an experiment on a real-world data set were conducted. The metrics used to evaluate filter performance are: (i) the RMS error, and (ii) the average normalized (state) estimation error squared (NEES) [7]. Specifically, for the landmarks we compute the average RMS and average NEES errors by averaging the squared errors and the NEES, respectively, over all Monte Carlo runs, all landmarks and all time steps. On the other hand, for the robot pose we compute these error metrics by averaging over all Monte Carlo runs for each time step (cf. [13] for a more detailed description).

The RMS of the estimation errors provide us with a concise metric of the accuracy of a given estimator. On the other hand, the NEES is a powerful metric for evaluating filter consistency. Specifically, it is known that the NEES of an M-dimensional Gaussian random variable follows a χ^2 distribution with M degrees of freedom. Therefore, if a certain filter is consistent, we expect that the average NEES for the robot pose will be close to 3 for all k, and that the average landmark NEES will be close to 2. The larger the deviations of the NEES from these values, the larger the inconsistency of the filter. By studying both the RMS errors and NEES of all the filters, we obtain a comprehensive picture of the estimators' performance.

4.1 Simulation

In the simulation tests presented in this section, the robot moves at a constant velocity of $v = 0.25$ m/sec, the standard deviation of the velocity measurement noise is equal to $\sigma_v = 0.1v$, while the rotational velocity measurements are corrupted by noise with standard deviation $\sigma_\omega = 1^o$/sec. The robot records measurements of the relative position of landmarks that lie within its sensing range of 5 m, with standard deviation equal to 15% of the robot-to-landmark distance along each axis. It should be pointed out that the sensor-noise levels selected for the simulations are larger than what is typically encountered in practice. This was done since larger noise levels lead to higher estimation errors, which in turn cause the Jacobian estimates to be less accurate, and make the effects of inconsistency more apparent.

In particular, a SLAM scenario with loop closure was considered where 100 Monte Carlo simulations were performed, and during each run, the robot executes 10 loops on a circular trajectory, and observes 20 landmarks in total. During the test, four filters process the same data, to ensure a fair comparison. The four filters compared are: (i) the ideal EKF, (ii) the standard EKF, (iii) the FEJ-EKF, and (iv) the robocentric filter [2, 3], which aims at improving the consistency of SLAM by expressing the landmarks in a robot-relative frame. The comparative results for all filters are presented in Fig. 1 and Ta-

Ideal EKF	Std EKF	FEJ-EKF	[2]
Robot Position Err. RMS (m)			
0.69	0.98	0.70	0.75
Robot Heading Err. RMS (rad)			
0.079	0.11	0.082	0.082
Robot Pose NEES			
3.05	12.79	3.68	6.70
Landmark Position Err. RMS (m)			
0.95	2.08	0.98	1.16
Landmark Position NEES			
2.1	12.93	2.35	6.65

Table 1. Robot Pose and Landmark Position Estimation Performance

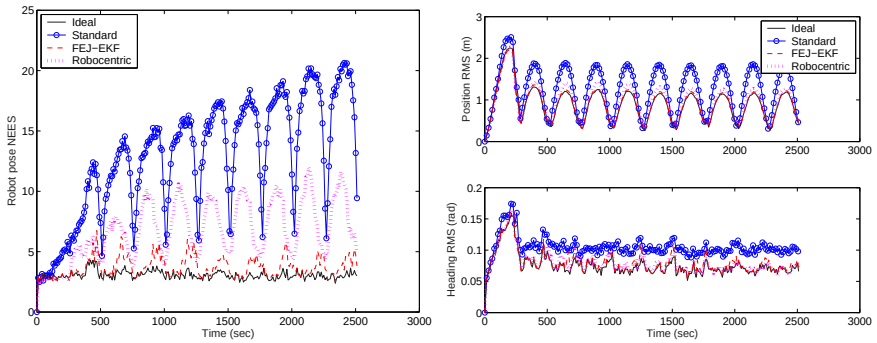

Fig. 1. Monte Carlo results for a SLAM scenario with multiple loop closures. (a) Average NEES of the robot pose errors (b) RMS errors for the robot pose (position and orientation). In these plots, the solid lines correspond to the ideal EKF, the dashed lines to the FEJ-EKF, the solid lines with circles to the standard EKF, and the dotted lines to the robocentric mapping algorithm of [2]. Note that the RMS errors of the ideal EKF and the FEJ-EKF are almost identical, which makes the corresponding lines difficult to distinguish.

ble 1. Specifically, Fig. 1(a) and Fig. 1(b) show the average NEES and RMS errors for the robot pose, respectively. On the other hand, Table 1 presents the average values of all relevant performance metrics for the landmarks and robot.

Several interesting conclusions can be drawn from these results. First, it becomes clear that the performance of the FEJ-EKF is *very close* to that of the ideal EKF, and substantially better than the standard EKF, both in terms of RMS errors and NEES. This occurs even though the Jacobians used in the FEJ-EKF are less accurate than those used in the standard EKF, as explained in the preceding section. This fact indicates that the errors introduced by the use of inaccurate Jacobians have a less detrimental effect on consistency than

the use of an error-state system model with observable subspace of dimension larger than that of the actual, nonlinear, SLAM system.

A second observation is that the FEJ-EKF also performs much better than robocentric mapping [2], both in terms of accuracy and in terms of consistency. One possible justification for this is that in robocentric mapping, during each propagation step *all* landmark position estimates need to be changed, since they are expressed with respect to the moving robot frame. As a result, during each propagation step (termed *composition* in [2]), all landmark estimates and their covariance are affected by the linearization errors of the process model. This problem does not exist in the world-centric formulation of SLAM, and it could offer an explanation for the observed behavior. As a final remark, we note that even though the FEJ-EKF NEES performance is significantly better compared to that of the robocentric mapping, the difference in the RMS errors of the two filters is less pronounced. This indicates that the effects of inconsistency primary affect the covariance, rather than the state estimates.

4.2 Experiment

To experimentally validate the performance of the FEJ-EKF, the filter was tested on the Sydney Car Park data set collected by Guivant and Nebot[2]. The experimental platform is a 4-wheeled vehicle equipped with a GPS, a laser sensor, and wheel encoders. The kinematic GPS system was used to provide ground truth for the robot position with 5 cm accuracy. Since the GPS has different frequency (up to 2 Hz) from the other exteroceptive sensors, we interpolated the GPS data to obtain the ground truth at each time step. Wheel encoders were used to provide odometric measurements, and propagation carried out using the Ackerman model. In this particular application, artificial landmarks were used that consisted of 60 mm steel poles covered with reflective tape. With this approach, it is easy to extract the features and the measurement model also becomes very accurate. Since the true position of the landmarks was also obtained with GPS, a true map was available for comparison purposes.

In this test, because the ground truth for the robot orientation was still unavailable, the ideal EKF could not be tested, and therefore the following three filters were compared: (i) the standard EKF, (ii) the FEJ-EKF, and (iii) the robocentric mapping filter [2]. The comparison results are shown in Table 2 and Figs. 2 and 3. Specifically, Table 2 presents the average values of all relevant performance metrics for the robot and the landmarks. On the other hand, Fig. 2 shows the trajectory and landmark estimates produced by the three filters, while Fig. 3 shows the NEES and RMS errors of the robot position over time. We point out that the NEES in this case pertains only to the robot position, and therefore the "optimal" value for it is 2.

These results demonstrate that the performance of the FEJ-EKF is better than the standard EKF and the robocentric mapping filter, both in terms of

[2] The data set is available: `www-personal.acfr.usyd.edu.au/nebot/dataset`

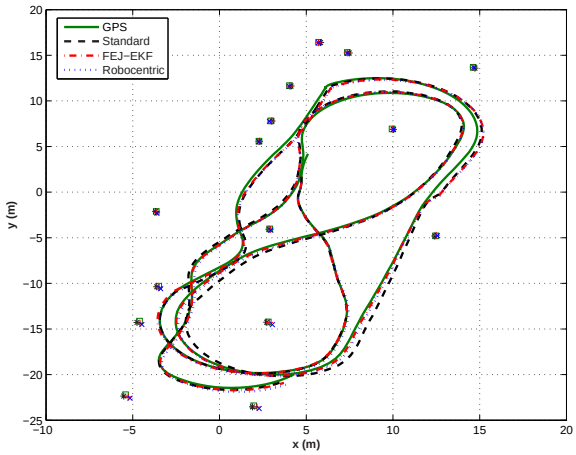

Fig. 2. The robot trajectory and landmark estimates. In this plot, the solid lines are ground truth obtained from GPS, while the boxes (□) are the known beacon positions. On the other hand, the dashed lines and crosses (+) are the estimated trajectory and landmarks corresponding to the standard EKF, the dash-dotted lines and stars (∗) correspond to the FEJ-EKF, and the dotted lines and x-crosses (×) to the robocentric mapping [2].

consistency and in terms of accuracy. In particular, the average RMS and the average NEES for the FEJ-EKF are better than the corresponding ones for the two competing filters. These results, along with those of the simulations presented in the previous section, lead us to the conjecture that the mismatch in the dimension of the unobservable subspace between the linearized SLAM system and the underlying nonlinear system is a fundamental cause of filter inconsistency.

Std EKF	FEJ-EKF	[2]
Robot Position Err. RMS (m)		
0.1002	0.0523	0.0838
Robot Position NEES		
2.8900	2.5197	2.8265
Landmark Position Err. RMS (m)		
0.3812	0.1858	0.2755
Landmark Position NEES		
2.5196	2.0197	2.4800

Table 2. Robot and Landmark Position Estimation Performance

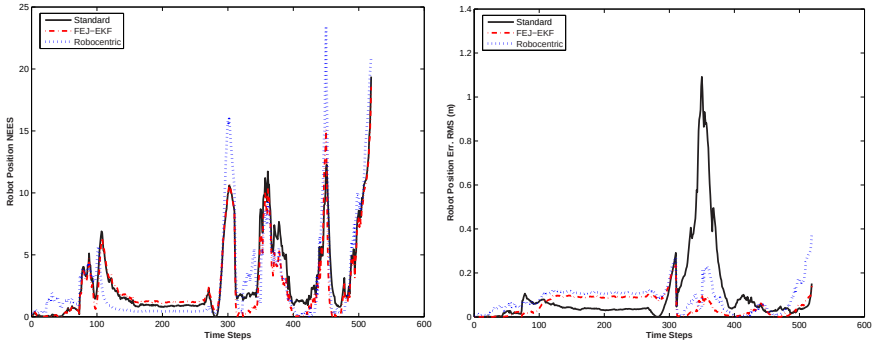

Fig. 3. (a) NEES of the robot position errors (b) RMS errors for the robot position. In these plots, the solid lines correspond to the standard EKF, the dash-dotted lines to the FEJ-EKF, and the dotted lines to the robocentric mapping algorithm of [2].

5 Conclusions

In this paper, we have studied in depth the issue of filter inconsistency in EKF-based SLAM. By comparing the observability properties of the nonlinear SLAM system model with those of the linearized error-state model employed in the EKF, we proved that the observable subspace of the standard EKF is always of higher dimension than the observable subspace of the underlying nonlinear system. As a result, the covariance estimates of the EKF undergo reduction in directions of the state space where no information is available, which is a primary cause of inconsistency. Based on the above analysis, a new "First Estimates Jacobian" (FEJ) EKF is proposed to improve the estimator's consistency during SLAM. The proposed algorithm performs better with respect to consistency, because when the filter Jacobians are calculated using the first available estimate for each state variable, the error-state system model has an observable subspace of the same dimension as the underlying nonlinear SLAM system. Through Monte Carlo simulations and experiments, we have verified that the FEJ-EKF is more accurate and more consistent than both the standard EKF and robocentric mapping [2], which has been proposed for improving estimator consistency in SLAM.

Acknowledgements

This work was supported by the University of Minnesota (DTC), and the National Science Foundation (EIA-0324864, IIS-0643680). Anastasios Mourikis was supported by the UMN Doctoral Dissertation Fellowship.

References

1. S. Julier and J. Uhlmann. A counter example to the theory of simultaneous localization and map building. In *IEEE International Conference on Robotics and Automation*, pages 4238–4243, Seoul, Korea, May 2001.
2. J.A. Castellanos, J. Neira, and J. Tardos. Limits to the consistency of EKF-based SLAM. In *5th IFAC Symposium on Intelligent Autonomous Vehicles*, pages 1244–1249, Lisbon, Portugal, July 2004.
3. J.A. Castellanos, R. Martinez-Cantin, J. Tardos, and J. Neira. Robocentric map joining: Improving the consistency of EKF-SLAM. *Robotics and Autonomous Systems*, 55(1):21–29, January 2007.
4. T. Bailey, J. Nieto, J. Guivant, M. Stevens, and E. Nebot. Consistency of the EKF-SLAM algorithm. In *IEEE/RSJ International Conference on Intelligent Robots and Systems*, pages 3562–3568, Beijing, China, Oct. 2006.
5. S. Huang and G. Dissanayake. Convergence analysis for extended Kalman filter based SLAM. In *IEEE International Conference on Robotics and Automation (ICRA)*.
6. S. Huang and G. Dissanayake. Convergence and consistency analysis for extended Kalman filter based SLAM. *IEEE Transactions on Robotics*, 23(5):1036–1049, Oct. 2007.
7. Y. Bar-Shalom, X.R. Li, and T. Kirubarajan. *Estimation with applications to tracking and navigation*. New York: Wiley, 2001.
8. J. Andrade-Cetto and A. Sanfeliu. The effects of partial observability in SLAM. In *IEEE International Conference on Robotics and Automation (ICRA)*, pages 394–402, New Orleans, LA, April 2004.
9. J. Andrade-Cetto and A. Sanfeliu. The effects of partial observability when building fully correlated maps. *IEEE Transactions on Robotics*, 21(4):771–777, August 2005.
10. K.W. Lee, W.S. Wijesoma, and J.I. Guzman. On the observability and observability analysis of SLAM. In *IEEE/RSJ Intenational Conference on Intelligent Robots and Systems (IROS)*, pages 3569–3574, Beijing, China, Oct. 2006.
11. R. Hermann and A. Krener. Nonlinear controllability and observability. *IEEE Transactions on Automatic Control*, 22(5):728 – 740, Oct. 1977.
12. G.P. Huang, A.I. Mourikis, and S.I. Roumeliotis. Analysis and improvement of the consistency of extended Kalman filter-based SLAM. In *IEEE International Conference on Robotics and Automation (ICRA)*, pages 473–479, Pasadena, CA, May 2008.
13. G. Huang, A. Mourikis, and S. Roumeliotis. Genearalized analysis and improvement of the consistency for EKF-based SLAM. Technical report, University of Minnesota, Minneapolis, MN, January 2008. www.cs.umn.edu/∼ghuang/paper/TR_slam_genconsistency.pdf.
14. Z. Chen, K. Jiang, and J.C. Hung. Local observability matrix and its application to observability analyses. In *16th Annual Conference of IEEE (IECON'90)*, pages 100–103, Pacific Grove, CA, Nov. 1990.
15. C. Meyer. *Matrix Analysis and Applied Linear Algebra*. SIAM, 2001.